

This document is the Accepted Manuscript version of a Published Work that appeared in final form in J. Mater. Chem. C, 2018, 6, 3968, copyright © Royal Society of Chemistry after peer review and technical editing by the publisher. To access the final edited and published work see [DOI: 10.1039/C8TC00840J].

Hydrogen-bonded azaphenacene: a strategy for the organization of π -conjugated materials.

Paula Gómez,^a Stamatis Georgakopoulos,^a José Pedro Cerón,^b Iván da Silva,^c Miriam Más-Montoya,^{a,d} José Pérez,^e Alberto Tárraga^a and David Curiel*^a

^a Department of Organic Chemistry, Faculty of Chemistry, University of Murcia, 30100-Murcia, Spain.

^b Bioinformatics and High Performance Computing Group, Universidad Católica San Antonio de Murcia (UCAM), Avda. Jerónimos, 135, 30107 Guadalupe, Murcia, Spain.

^c ISIS Facility, STFC Rutherford Appleton Laboratory, Chilton, Oxfordshire OX11 0QX, United Kingdom.

^d Molecular Materials and Nanosystems, Institute for Complex Molecular Systems, Eindhoven University of Technology, P.O. Box 513, 5600 MB Eindhoven, The Netherlands.

^e Department of Mining, Geological y Cartographic Engineering, Technical University of Cartagena, 30203 Cartagena, Spain.

Electronic Supplementary Information (ESI) available: OFET fabrication and characterization, ¹H-NMR and ¹³C-NMR spectra, TGA, DSC, TD-DFT, Rietveld refinement, CCDC 1557392.

A centrosymmetric fused polyheteroaromatic system, namely 7-azaindolo[2,3-*h*]α-carboline has been synthesized. The pentacyclic structure includes rationally located hydrogen bond donor and hydrogen bond acceptor sites to induce its self-assembly. The molecular units associate forming an extended monodimensional arrangement that further self-organizes through π -stacking. The optical, electrochemical, X-ray diffraction, computational and electronic characterization in organic field effect transistors proves the utility of hydrogen bond-directed self-assembly as strategy to enhance edge-to-edge interactions and orbital overlap that contribute to the charge transport properties in π -conjugated systems.

Introduction

Conjugated systems with a π -extended structure have gained much attention due to their utility as semiconductors for the fabrication of future generations of electronic devices.¹⁻¹⁰ The synthesis of fused polyaromatic and polyheteroaromatic molecules actively contributes to the progress of this topic by supplying a countless variety of materials seeking for an optimization of the required optical, electronic and morphological properties.^{11, 12} A compromise between these three features will ultimately determine the ability of organic materials to transport charge carriers. The molecular structure has a remarkable influence on the semiconducting properties of the materials processed as solid thin-films. In this regard, charge transport in organic semiconductors follows an intermolecular hopping mechanism which, according to the semiclassical theory of electron transfer, depends on the orbital overlap and the reorganization energy.¹³⁻¹⁵ In turn, these parameters can be modulated by adequate synthetic modifications on the conjugated molecules. Accordingly, a deeper knowledge about the correlation between molecular structure, solid state arrangement and charge transport currently represents one of the important objectives that could contribute to the design of better organic materials. Extensive work has been particularly done to find structure-property connections between the solid state packing and the charge transport properties.^{16, 17} Some packing patterns have been more commonly observed in polyaromatic and polyheteroaromatic systems (herringbone, cofacial columnar stacking, slipped-stacking and brick layer packing) (Fig. 1). Herringbone structure has revealed as an excellent molecular arrangement since very high charge mobilities have been reported in OFETs where the semiconductor adopted this packing.^{18, 19} This is attributed to the right orientation of the molecules on the substrate that enables a 2D transport parallel to the substrate surface.²⁰ The herringbone pattern is frequently observed in acenes and heteroacenes.^{21, 22} Nevertheless, the relative orientation of the molecules in a herringbone packing causes displacements along their short axis resulting in a reduced π - π stacking. Since it has been demonstrated that maximization of face-to-face interactions improves charge transport, continuous efforts have been done with the aim of enhancing π - π stacking in fused polyaromatic molecules.²³ Generally, the other three mentioned packing modes show larger surface overlap. In the case of the columnar arrangement, whereas the cofacial packing will improve charge transport within the columns, this can accentuate the transport anisotropy. Therefore, charge hopping between adjacent columns will depend on the intermolecular electronic coupling in that particular direction, which can be conditioned by the tilt between neighbor columns. Alternatively, when molecules order in parallel planes the slipped-stacking and bricklayer modes are defined. These two packing configurations are normally characterized by the relative shift between parallel layers. Again, the transport out of the stacking direction is usually hindered. In any case, it is important to realize that, for an overall analysis of the crystal

packing in polyaromatic systems, the packing mode should be observed along the short and long axis of the molecule, since different packing patterns could be adopted depending on the orientation of the molecule.

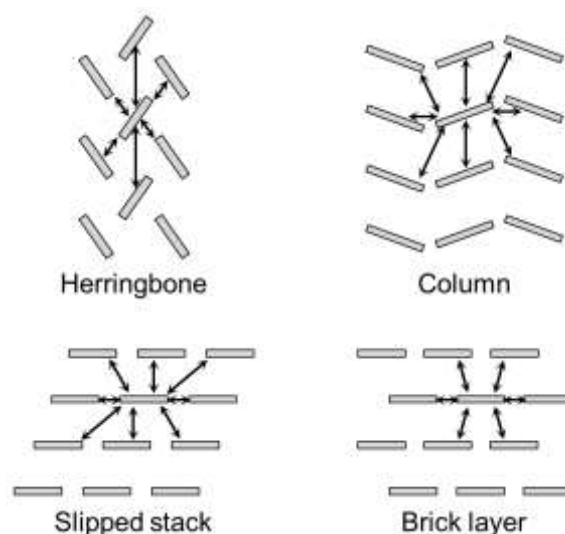


Fig. 1 Frequent packing modes observed in molecular crystals. Arrows represent the possible directions for charge transport.

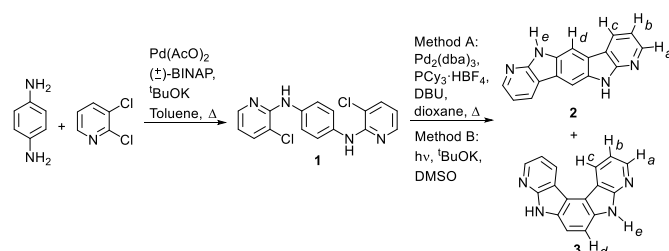
The synthetic strategies that have been followed to explore the modulation of π - π interactions basically consist in the peripheral functionalization of the acene or heteroacene cores.²⁴⁻³¹ Nevertheless, the driving force for the solid state packing in these molecules will mainly be due to very weak π - π interactions,³² with the assistance of sulphur-sulphur interactions in the case of the thienoacene derivatives.^{33, 34} The weakness of these interactions makes it very difficult to control and/or predict the packing mode from the molecular structure, with minor structural changes sometimes leading to packing modes difficult to anticipate. Currently, the research in computational chemistry explores different methods that can be used to explain the correlation between molecular structure, crystal packing, supramolecular interactions and charge transport parameters.³⁵⁻³⁸ However the combination of so many different features and the weak dispersive character of the interactions governing the solid state arrangement of π -conjugated systems limit the predictive ability of the theoretical procedures so far. In this context, it might be worth considering that if stronger non-covalent interactions such as hydrogen bonding could intervene, this would induce a higher degree of organization by the strategic location of interacting sites in the molecules. Subsequently, this approach could lead to more stable solid structures by spontaneous self-assembly.^{39, 40} Although this concept is ubiquitous in the organization of biological systems and is exploited in the discipline of crystal engineering,⁴¹ it can also be valuable to further explore it in the area of organic electronics.^{42, 43} An approach based on the use of intramolecular hydrogen bonding has reported the benefits of this strategy in the planarization of conjugated systems that subsequently promotes the aggregation of coplanar conformers through strong π - π stacking interactions.⁴⁴ Concerning the use of intermolecular hydrogen bond-directed assembly, peripheral substituents with hydrogen bonding functions are normally attached to the conjugated system to promote the self-assembly.⁴⁵ However, those side substituents can interfere with the charge transport process between the packed conjugated cores whose contact plays a key role. Alternatively, some molecules have been reported where self-assembly is directed through hydrogen bonds established by the conjugated system itself.⁴⁶⁻⁵¹ Nevertheless, the structure of these molecules occasionally presents discontinuities in the conjugated structure. Based on these precedents, we report the synthesis and characterization of a pentacyclic system, with a fully through-conjugated structure, that has been rationally designed to self-assemble through the hydrogen bond donor and acceptor sites of the 7-azaindole unit. Trying to anticipate what the solid structure might look like, a centrosymmetric structure was defined as the synthetic objective to achieve a linear aggregation. The hydrogen-bonded aggregates are intended to form an expanded π -surface that will favour a secondary assembly *via* π - π stacking and could further enable the intermolecular charge transport. This conducts us to the unprecedented structure of pyrido[2,3-*b*]pyrido[3',2':4,5]pyrrolo[2,3-*f*]indole, **2**, whose nomenclature will be simplified as 7-azaindolo[2,3-*h*] α -carboline (Scheme 1).

Results and discussion

Synthesis and characterization

The synthetic route for this molecule comprises two steps. Initially, a double *N*-arylation of *p*-phenylenediamine with 2,3-dichloropyridine produces *N,N'*-bis(3-chloropyridin-2-yl)*p*-phenylenediamine, **1**. Subsequently, two different methods have been used to cyclize compound **1** and obtain the pentacyclic system. Firstly, a palladium catalyzed aryl-heteroaryl cross-coupling reaction involving C-H and C-Cl bonds was applied.⁵² Since this required prolonged heating in a sealed tube, we also explored a

more straightforward alternative. Thus, we used a photochemically induced double intramolecular radical nucleophilic aromatic substitution.⁵³ This reaction proceeds smoothly, producing the same result as the above mentioned thermal treatment but in less than two hours. As expected, according to the geometry of compound **1**, the crude solid obtained by both methods contained a mixture of regioisomers, namely 7-azaindolo[2,3-*h*]α-carboline, **2**, and 7-azaindolo[3,2-*g*]α-carboline, **3**, in approximately 1:1 ratio.



Scheme 1 Synthesis of 7-azaindolo[2,3-*h*]α-carboline, **2**.

Since our synthetic objective focused on the isolation of compound **2**, considering the very low solubility of the products, the purification was achieved by several cycles of gradient sublimation. The less volatile fractions, which were enriched with isomer **2**, were collected, combined and resublimed until a total of five sublimation experiments to isolate **2** as a pure product (Fig. S2).

Due to the similar aspect expected for the NMR spectra of both regioisomers, the identity of compound **2** was unequivocally confirmed by NOESY experiments (Fig. 2). Thus, focusing on the singlet at 8.20 ppm, ascribed to proton H_d , this peak shows 2D-correlation with two more peaks, namely, the singlet at 11.71 ppm ascribed to the NH proton (H_e) and the doublet of doublets at 8.60 ppm ascribed to proton H_c , evidencing the spatial proximity between these nuclei. As it could be inferred from the structures of **2** and **3**, isomer **2** was the only one where the described NOE correlations could simultaneously happen. Therefore, the remaining NOESY signals $H_a \leftrightarrow H_b$ and $H_b \leftrightarrow H_c$, in combination with the $^1\text{H-NMR}$ and $^{13}\text{C-NMR}$ data, confirmed the assignment of the peaks and the structure of the isolated 7-azaindolo[2,3-*h*]α-carboline, **2**.

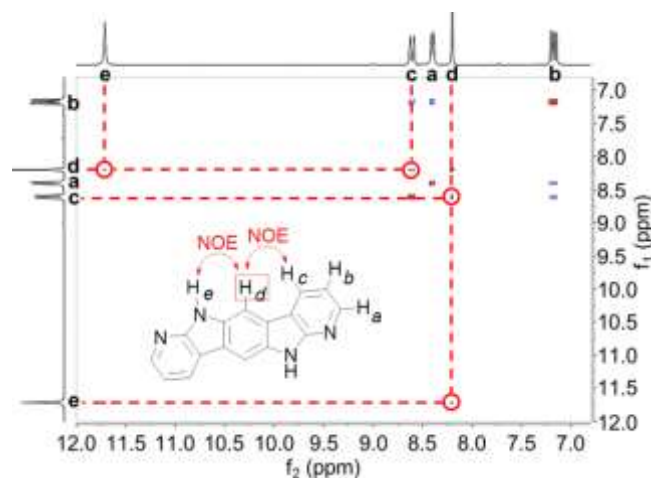


Fig. 2 NOESY spectrum of compound **2**.

Additionally, thermal characterization of compound **2** was carried out by thermogravimetric analysis (TGA) and differential scanning calorimetry (DSC) (Fig. S4). The TGA did not show any significant mass loss (5%) up to 363°C and the DSC results did not evidence any phase transition within the range 70-300°C, proving the thermal stability of the molecular material.

Electronic structure

The electronic structure of compound **2** was determined by combining cyclic voltammetry, UV-vis spectroscopy and Density Functional Theory (DFT) methods (Fig. 3). Concerning the electrochemical characterization, the surface of the working electrode was coated by drop casting a suspension of the molecule in THF. The resulting voltammogram displayed an irreversible wave. Using the onset of the oxidation process (0.87 V) and a reference potential to set the energy with respect to the vacuum level, a HOMO energy of -5.5 eV was estimated.^{54, 55} This low lying HOMO should confer stability towards ambient oxidation on the 7-azaindolo[2,3-*h*]α-carboline, **2**.

The absorption spectrum in solution showed two intense bands at 277 nm ($\epsilon \approx 3 \times 10^4 \text{ cm}^{-1} \text{ M}^{-1}$) and 344 nm ($\epsilon \approx 7 \times 10^4 \text{ cm}^{-1} \text{ M}^{-1}$), and a set of weak bands at lower energies (375-415 nm). All these bands correspond to $\pi\text{-}\pi^*$ transitions typical of the β , p

and α bands (from higher to lower energy) defined by the Clar theory of fused polyaromatic systems.⁵⁶ The assignment of these bands was additionally corroborated by computational methods using Time Dependent-DFT (TD-DFT) calculations (Fig. S5). Besides, the absorption spectrum in the solid state was measured for a thin film showing the red shift coming from the intermolecular interactions in a solid state sample. The onset of the later spectrum at 490 nm, is ascribed to the $S_0 \rightarrow S_1$ transition, which is related to the energy difference between HOMO and LUMO. Thus, the LUMO energy (-3 eV) was calculated from the difference between the optical gap (2.5 eV) and the HOMO energy previously determined. These energies are in good agreement with the frontier orbitals assessed by computational methods that also showed how the distribution of HOMO and LUMO spread all over the conjugated structure of the molecule, benefitting charge delocalization. The emissive properties of compound **2** were also studied by fluorescence spectroscopy. A short Stokes shift (18 nm) was observed as normally happens for polyaromatic molecules having a rigid structure. Moreover, a low quantum yield (5 %) was measured.

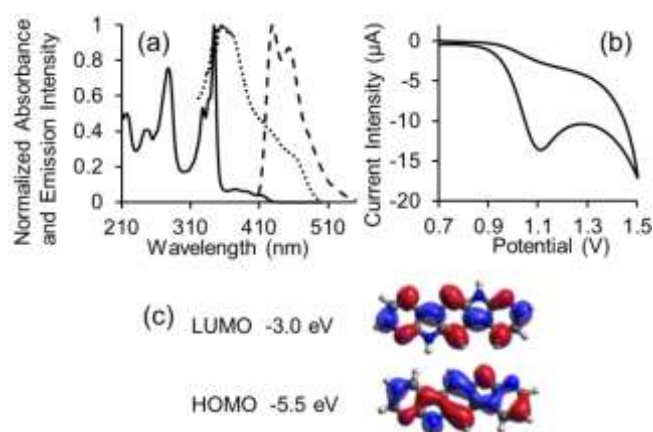


Fig. 3 Characterization of **2**: (a) Absorption (continuous plot) and emission (dashed plot) spectra (THF, [2]= 5×10^{-5} M). Solid thin film absorption (dotted plot); (b) Cyclic voltammetry; (c) HOMO and LUMO energies and isosurface.

Solid state packing

Powder X-ray diffraction (XRD) experiments (Table S1, and Fig. S6) revealed the solid state packing of the molecule and confirmed the objective of inducing a hydrogen bond-directed self-assembly (Fig. 4). Compound **2** crystallizes in a triclinic lattice where every molecule of 7-azaindolo[2,3-*h*]α-carboline forms four hydrogen bonds with two neighbor molecules owing to the mutual interactions between the 7-azaindole units ($N-H \cdots N = 2.8 \text{ \AA}$, distance between nitrogen atoms).⁵⁷

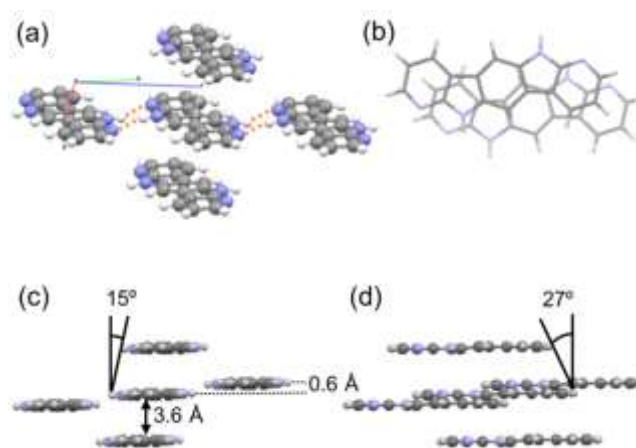


Fig. 4 X-ray structure of compound **2**. Molecules in van der Waals contact (a); projections of molecular packing across the π -stacking direction (b). long axis (c) and short axis (d).

This arrangement results in an extended linear assembly where molecules are not coplanar but form very short steps 0.6 Å high. These steps are caused by the packing of parallel π -stacks, resembling the proposed structure for another hydrogen bonded molecule such as α -quinacridone polymorph.⁵⁸ Stacked molecules show an interplanar distance of 3.6 Å and present pitch and roll angles of 27° and 15° derived from a slight slipping of 1.4 Å and 1.3 Å along their long and short axis respectively. This little displacement of stacked molecules allows a significant overlap of the aromatic systems which subsequently favors intermolecular orbital interactions as it will be discussed later.⁵⁹

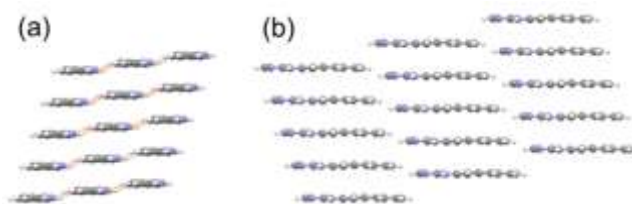


Fig. 5 Slipped-stacking view (a) across the long axis (orange lines represent hydrogen bonds) and (b) across the short axis.

An expansion of the crystalline network shows that the molecular arrangement corresponds to a unique slipped-stacking since this packing mode is observed both for the projections across the long and short molecular axis. Molecules pile up in parallel planes forming columns. In turn, stacked molecules also remain parallel with respect to other molecules packed in adjacent columns. The projection of this columnar arrangement across the long axis of the 7-azaindolo[2,3-*h*]α-carboline evidences hydrogen bonds established through the 7-azaindole units that support the edge-to-edge interactions (Fig. 5a). This disposition is also observed for the projection of the columns across the short molecular axis where edge-to-edge (short end-to-short end) intercolumnar interactions are established through the extreme C-H bonds (Fig. 5b).

Hirshfeld surfaces have been calculated to analyze the supramolecular interactions in the solid state (Fig. 6).^{60, 61} Accordingly, red spots associated to intense interactions clearly manifest on the hydrogen bond donor (NH_{pyrrole}) and hydrogen bond acceptor (N_{pyridine}) sites. Besides, white regions, corresponding to less intense interactions such as face-to-face π-π stacking, are observed on both sides of the plane defined by the pentacyclic system. White spots can also be detected on the short side of the molecule depicting the edge-to-edge interactions with molecules packed in adjacent stacks.

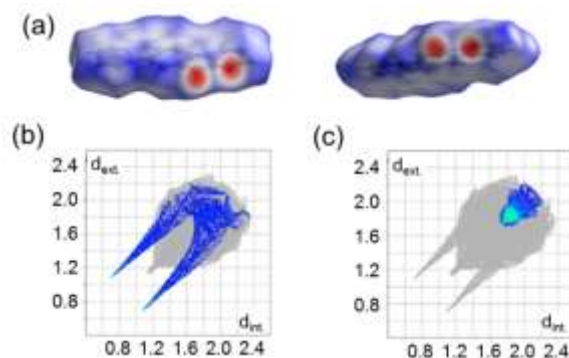


Fig. 6 (a) Front and back views of Hirshfeld surface. 2D fingerprints: (b) H...N interactions and (c) C...C interactions.

The representation of the distance from the Hirshfeld surface to the external surrounding atoms vs. internal atoms gives a 2D-fingerprint where a specific type of interaction can be displayed.^{62, 63} Regarding the interactions established by compound **2**, the H...N hydrogen bonds cover a significant surface of the 2D-plot in a range between 2.2 Å and 0.7 Å and show the typical spike shape of hydrogen bonding. The C...C interactions are mainly ascribed to the π-π stacking and concentrate in a narrower range of distances (1.8-2.2 Å). Importantly, the greenish area centered at 1.8 Å indicates that a higher concentration of interacting points exists, evidencing the previously mentioned large intermolecular overlap. Moreover, the sum of the internal and external distances (approximately 3.6 Å) matches well the interplanar distance, previously determined by XRD, between stacked molecules.

Charge transport and thin film morphology

The charge transport in compound **2** was studied in Organic Field-Effect Transistors (OFETs) with a bottom gate-top contact architecture (Si/SiO₂ (300 nm)/Polystyrene (33 nm)/Compound **2** (50 nm)/MoO₃ (9 nm)/Au_{source & drain} (40 nm)) prepared by thermal evaporation, without any substrate heating or thin film annealing. The polystyrene layer coating the SiO₂ was used to attenuate the possible effect of interfacial dipoles⁶⁴ and the MoO₃ interfacial layer improves hole injection from the gold electrode into a semiconductor with a low lying HOMO, such as compound **2**.^{65, 66} A hole mobility of $1.3 \times 10^{-3} \text{ cm}^2 \text{ V}^{-1} \text{ s}^{-1}$ was extracted from the transfer characteristics (Fig. 7).

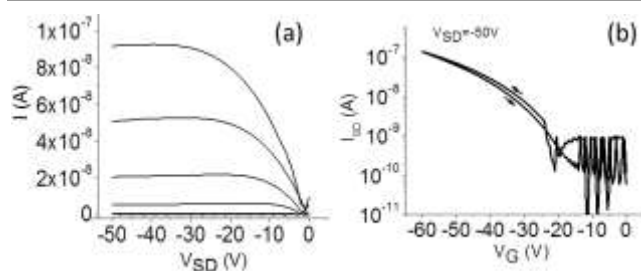


Fig. 7 (a) Output ($V_G = 0$ to $-60V$; step $-10V$) and (b) transfer characteristics of the OFETs fabricated with compound **2**.

The AFM images of the organic semiconducting thin film showed that it was constituted by tangled fibers and it had a root mean square (rms) roughness of 0.4 ± 0.1 nm (Fig. 8a). Besides, X-ray diffraction experiments carried out on the same samples revealed that, due to the absence of diffraction peaks (Fig. 8b), the morphology essentially corresponded to a non-crystalline film or a film without a long range preferential molecular orientation on the substrate surface.

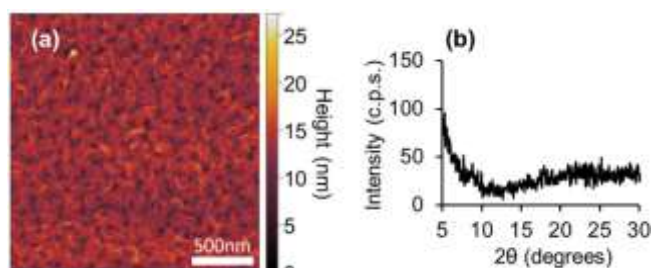


Fig. 8 Evaporated thin film of compound **2**: (a) AFM image and (b) X-ray diffractogram.

Interestingly, the characterization data reveal that, despite the lack of crystallinity in the thin films, the charge mobility reached by compound **2** is quite high for an amorphous material.⁶⁷⁻⁶⁹ A reliable comparison with analogous OFETs fabricated with a molecule that displays very similar slipped-stacked packing and morphology, such as the broadly studied 6,13-bis((triethylsilyl)ethynyl)pentacene (TES-pentacene), shows that compound **2** presents a hole mobility two orders of magnitude higher.^{28, 70}

Thus, with the aim of getting a better understanding of these results, computational studies using DFT experiments were done. Charge transport in organic solids is favored by the intermolecular orbital overlap that can be quantified by the calculation of the transfer integrals. Accordingly, based on the above described solid state packing, the surface intersection between π -stacked molecules, along with the distribution of the HOMO orbital, results in a transfer integral value of 145 meV (Fig. 9). Considering that the electronic coupling exponentially decays with the π - π stacking distance⁷¹ and that **2** displays a longer stacking distance than TES-pentacene, the magnitude of the face-to-face transfer integrals in **2** is high, strengthening the adequacy of the molecular design.²⁴ Besides, the hydrogen bond network defined by 7-azaindolo[2,3-*h*]α-carboline, **2**, stabilizes the expansion of the π -surface in the form of linear strips. As a consequence, the larger surface of self-assembled strips reinforces the π - π interactions leading to an environment where charge transport in the stacking direction would be highly favored. On the other hand, quite commonly, molecules packed in a slipped-stack mode present very low charge transfer integral values along the edge-to-edge direction. Sometimes, due to the steric hindrance of peripheral substituents, edge-to-edge interactions are even non-existent and charge transport along that direction is negligible.²¹ However, in the case of 7-azaindolo[2,3-*h*]α-carboline, **2**, the transfer integrals between hydrogen-bonded molecules reach a value of 15 meV, which probes how edge-to-edge interactions can be enhanced via hydrogen-bonding.^{72, 73} Consequently, that will probably improve charge transport along that direction. In agreement with these results, the electronic coupling determined for 7-azaindolo[2,3-*h*]α-carboline, **2**, would explain the high mobility observed in an amorphous film without long range order.

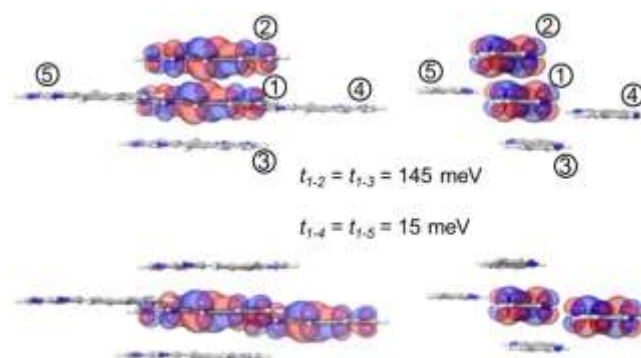


Fig. 9 Calculated transfer integrals (t_{ab}) and HOMO isosurfaces of compound **2**. Two views of the π -stacked (top) and hydrogen bonded (bottom) isosurfaces.

Therefore, although the slipped-stack packing in compound **2** would still present an anisotropic charge transport, this can be partially attenuated by the intermolecular interactions reinforced through hydrogen bond-directed self-assembly. This approach proves how the strategic use of strong non-covalent interactions can govern the solid-state organization of conjugated systems and improve their charge transport parameters. Accordingly, the reported results offer a new structural alternative for the development of supramolecular electronics.

Conclusions

In summary, a simple synthetic methodology has been optimized for the azaphenacene 7-azaindolo[2,3-*h*] α -carboline. This molecule has an innovative structure that incorporates hydrogen bond donor and acceptor sites into the polyheteroaromatic system without disrupting its conjugation. The solid state packing of the molecule defines hydrogen-bonded monodimensional assemblies that contribute to extend the π -conjugated surface of the molecular material and subsequently favor π -stacking. This results in good transfer integrals along both face-to-face and edge-to-edge directions that explain the charge transport observed in organic field-effect transistors where the 7-azaindolo[2,3-*h*] α -carboline has been used as organic semiconductor.

Experimental

N,N'-Bis(3-chloropyridin-2-yl)*p*-phenylenediamine, **1**

A round bottom flask was charged with (\pm)-BINAP (0.68g, 7.5 mol %), dry toluene was added (50 mL) and the mixture was heated under nitrogen atmosphere until a clear solution was obtained. Then Pd(OAc)₂ (0.17 g, 5 mol %) was added and the solution was stirred for fifteen minutes. A second round bottom flask was charged with *p*-phenylenediamine (1.56 g, 14.7 mmol), 2,3-dichloropyridine (5 g, 33.8 mmol), potassium *tert*-butoxide (4.95 g, 44.1 mmol) and dry toluene (20 mL) under inert atmosphere. The solution of the palladium catalyst was transferred to the second flask *via* syringe and the resulting mixture was heated under reflux temperature for 24 hours. The reaction was allowed to cool down and was quenched with water. The organic phase was washed with water (3x30 mL) and then dried with anhydrous Na₂SO₄. Afterwards, the solution was filtered and the solvent was evaporated under reduced pressure. Finally, the crude product was purified by liquid chromatography, using silica gel as stationary phase and dichloromethane as eluent. The fractions containing the desired product were evaporated under reduced pressure and the resulting solid was triturated with methanol to obtain an analytically pure yellow product (3.19 g, 66 %). M. p.: 130-132 °C. ¹H-NMR (200 MHz, CDCl₃), δ (ppm): 8.11 (dd, 2H, py, *J*=4.8, 1.6 Hz), 7.59 (s, 4H, Ph), 7.55 (dd, 2H, py, *J*=7.8, 1.6 Hz), 6.93 (s, 2H, NH), 6.67 (dd, 2H, py, *J*=7.8, 4.8 Hz). ¹³C-NMR (50 MHz, CDCl₃), δ (ppm): 151.5, 145.8, 136.5, 134.8, 121.1, 115.8, 114.8. HRMS (*m/z*): (C₁₆H₁₃Cl₂N₄); Found: 331.0519 (M+H)⁺; Calculated: 331.0512.

7-Azaindolo[2,3-*h*] α -carboline, **2**

Method A: A solution of Pd₂(dba)₃ (0.28 g, 20 mol %) and PCy₃·HBF₄ (0.22 g, 40 mol %) in dry 1,4-dioxane (20 mL) was stirred for fifteen minutes under nitrogen atmosphere. Then, this solution was added over another solution of compound **1** (0.5 g, 1.51 mmol) and DBU (0.9 mL, 6.04 mmol) in dry dioxane (20 mL). The mixture was transferred to a sealed tube maintaining the inert atmosphere, and this was heated at 200 °C for 24 hours. After this time, the reaction was allowed to cool down to room temperature and it was poured on a beaker containing water (50 mL). The resulting precipitate was filtered and washed with methanol (4x15 mL) to obtain 0.33 g of crude solid.

Method B: A photochemical reactor was loaded with DMSO (160 mL), potassium *tert*-butoxide (0.81 g, 4.53 mmol) and compound **1** (0.6 g, 1.81 mmol), under continuous nitrogen flow. After degassing for 10-15 minutes, the reaction mixture was irradiated with a medium-pressure mercury lamp for 2.5h. Afterwards, the reaction was allowed to cool down to room

temperature and was poured into a saturated solution of ammonium chloride (100 mL). The resulting precipitate was filtered and washed with methanol (3x30 mL) to obtain 0.37 g of a crude solid.

The crude solid (0.6 g) obtained from either method A or B was purified by gradient sublimation under high vacuum ($T = 215$ °C; $P = 10^{-6}$ mbar). The less volatile fractions were collected, combined and resublimed until a total of five sublimation experiments were completed to isolate compound **2** as a pure product (0.15 g, 25%) (Figures S2 and S3). M. p.: >300 °C. $^1\text{H-NMR}$ (200 MHz, DMSO-d_6), δ (ppm): 11.71 (s, 2H, NH), 8.60 (dd, 2H, py, $J = 7.7, 1.5$ Hz), 8.40 (dd, 2H, py, $J = 4.8, 1.5$ Hz), 8.20 (s, 2H, Ph), 7.17 (dd, 2H, py, $J = 7.7, 4.8$ Hz). $^{13}\text{C-NMR}$ (75 MHz, DMSO-d_6), δ (ppm): 153.0, 146.1, 134.0, 128.5, 120.9, 115.5, 114.4, 102.3. HRMS (m/z): ($\text{C}_{16}\text{H}_{11}\text{N}_4$); Found: 259.0976 ($\text{M}+\text{H}^+$); Calculated: 259.0978.

Structural characterization

$^1\text{H-NMR}$ and $^{13}\text{C-NMR}$ spectra were recorded on spectrometers having frequencies of 200 MHz or 300 MHz for proton nuclei and 50 MHz or 75 MHz for carbon nuclei, respectively. Chemical shifts are referred to the residual peak from the deuterated solvent. Mass spectrometry was recorded on HPLC-MS TOF 6220 instrument.

Thermal characterization

Thermogravimetric analysis was carried out on a SDT 2960 analyzer from TA Instruments at a heating rate of 10 °C min^{-1} under nitrogen. Differential Scanning Calorimetry analysis was carried out on a TA Instrument DSC 2920.

Optical and electrochemical characterization

Absorption spectra were recorded on a Cary 5000 UV-vis-NIR spectrophotometer. Emission spectra were recorded on a Cary Eclipse spectrophotometer ($\lambda_{\text{exc.}} = 344$ nm). Quantum yields were measured using a calibration plot built with anthracene standard covering the concentration range 3×10^{-5} M to 3×10^{-6} M in ethanol.

Cyclic voltammetry was recorded utilizing a BioLogic SP-200 potentiostat and using boron doped diamond electrode as working electrode, platinum wire as counter-electrode and Ag/AgCl as reference electrode at a scan rate of 100 mVs^{-1} . The supporting electrolyte was tetrahexylammonium hexafluorophosphate (0.1 M) in acetonitrile. The HOMO levels were estimated, without considering any solvent effect, from the onset potentials of oxidation wave respect to the energy level of the ferrocene/ferrocenium redox couple used as internal reference.

X-ray diffraction and thin film morphology

Powder X-ray diffraction: High resolution powder X-ray diffraction patterns were measured at the ESRF synchrotron (Grenoble, France) using the Spanish beamline SpLine (BM25A) with a 0.56523 Å wavelength, at room temperature. Sample was loaded in a borosilicate capillary tube and mounted on a rotatory goniometric head, to reduce the effect of possible preferential orientations. Measurement was performed in a 2θ continuous scan mode, with a 0.004° effective step. The incident beam (dimensions: 10 mm horizontal x 0.5 mm vertical) was monitored to normalize the collected data considering the primary beam decay. The diffracted beam was collected using a point detector. Data was measured within a $3\text{--}32^\circ$ 2θ range, corresponding to a 1.03 Å resolution. The structure of compound **2** was solved ab initio and refined using Rietveld method with Topas Academic 5 program (<http://www.topas-academic.net/>). The final Rietveld plot is given in Fig. S6. Crystallographic parameters are summarized in Table S1.

Thin film X-ray Diffraction: Data were collected on a Bruker D8 Advance instrument in $\theta\text{--}\theta$ mode with $\text{CuK}\alpha$ radiation (wavelength 1.54060 Å), 40 kV, 30 mA, and a 1-dimensional detector with a window of 1° . Primary optics consisted of a 2° Soller slit, a 1 mm incidence slit, and an air scatter screen. Secondary optics included a 3 mm antiscatter slit, a Ni filter and a 2.5° Soller slit. Sample was step scanned from 3 to 65° in 2θ , with 0.05° stepping intervals, 0.1 s per step, and a rotation speed of 30 rpm.

AFM measurements were performed on a NT-MDT microscope (NTEGRA PRIMA) in tapping mode and images were analyzed with Gwyddion V2.47.

Computational calculations

The theoretical treatment of the molecules was based on density functional theory (DFT) methods. The reorganization energy (λ) was first computed by optimizing the molecular structure both in its neutral and cationic states at B3LYP/6-311++G(d,p) level⁷⁴ as implemented in Jaguar^{75, 76}. This functional has demonstrated its accuracy to predict reorganization energies in OFETs.⁷⁷ The reorganization energy, combined with data of the X-ray structure, was subsequently used to calculate the transfer integrals (t_{ab}). Long-range-corrected (LC) DFT has been used for the assessment of transfer integrals reducing the variability due to the amount of Hartree-Fock exchange included in the functional at the theoretical stage of material design.⁷⁸ In the present contribution, we used the Baer–Neuhauser–Livshits (BNL) functional,^{79, 80} which correctly conduct such calculations within the LC approach.⁸¹ In our case, the previously reported CDFT formulation has been used as implemented in the Material Science Suite of Schrödinger.^{82, 83} As shown in Fig. 9, the transfer integrals were computed by using a 5 molecules model, which has been designed by including a reference molecule located at the unit cell and all surrounding molecules. The graphical processing of the computational calculations was done with Maestro 2016-4.⁸⁴

Conflicts of interest

There are no conflicts of interest to declare.

Acknowledgements

Authors are grateful for the financial support from the Spanish Ministry of Economy and Competitiveness (CTQ2014-58875) and from Fundación Séneca (19419/PI/14-1). Authors also acknowledge the Spanish Ministry of Economy and Competitiveness and Consejo Superior de Investigaciones Científicas for financial support and for provision of synchrotron radiation facilities. Besides, authors thank E. Salas-Colera for his assistance in using beamline BM25-SpLine at the ERSF Synchrotron in Grenoble (France).

Notes and references

1. W. Chen and Q. Zhang, *J. Mater. Chem. C*, 2017, **5**, 1275-1302.
2. F. Würthner, C. R. Saha-Möllner, B. Fimmel, S. Ogi, P. Leowanawat and D. Schmidt, *Chem. Rev.*, 2016, **116**, 962-1052.
3. M. Gsänger, D. Bialas, L. Huang, M. Stolte and F. Würthner, *Adv. Mater.*, 2016, **28**, 3615-3645.
4. C. Wang, P. Gu, B. Hu and Q. Zhang, *J. Mater. Chem. C*, 2015, **3**, 10055-10065.
5. J. Li and Q. Zhang, *ACS Appl. Mater. Interfaces*, 2015, **7**, 28049-28062.
6. Q. Ye and C. Chi, *Chem. Mater.*, 2014, **26**, 4046-4056.
7. Q. Miao, *Adv. Mater.*, 2014, **26**, 5541-5549.
8. W. Jiang, Y. Li and Z. Wang, *Chem. Soc. Rev.*, 2013, **42**, 6113-6127.
9. C. Wang, H. Dong, W. Hu, Y. Liu and D. Zhu, *Chem. Rev.*, 2011, **112**, 2208-2267.
10. T. M. Figueira-Duarte and K. Müllen, *Chem. Rev.*, 2011, **111**, 7260-7314.
11. J. Mei, Y. Diao, A. L. Appleton, L. Fang and Z. Bao, *J. Am. Chem. Soc.*, 2013, **135**, 6724-6746.
12. H. Dong, X. Fu, J. Liu, Z. Wang and W. Hu, *Adv. Mater.*, 2013, **25**, 6158-6183.
13. N. Tessler, Y. Preezant, N. Rappaport and Y. Roichman, *Adv. Mater.*, 2009, **21**, 2741-2761.
14. V. Coropceanu, J. r. m. Cornil, D. A. da Silva Filho, Y. Olivier, R. Silbey and J.-L. Brédas, *Chem. Rev.*, 2007, **107**, 926-952.
15. R. A. Marcus, *Rev. Mod. Phys.*, 1993, **65**, 599-610.
16. C. Wang, H. Dong, L. Jiang and W. Hu, *Chem. Soc. Rev.*, 2018, **47**, 422-500.
17. M. Mas-Torrent and C. Rovira, *Chem. Rev.*, 2011, **111**, 4833-4856.
18. M. Watanabe, Y. J. Chang, S.-W. Liu, T.-H. Chao, K. Goto, M. M. Islam, C.-H. Yuan, Y.-T. Tao, T. Shinmyozu and T. J. Chow, *Nat. Chem.*, 2012, **4**, 574.
19. H. Minemawari, T. Yamada, H. Matsui, J. y. Tsutsumi, S. Haas, R. Chiba, R. Kumai and T. Hasegawa, *Nature*, 2011, **475**, 364.
20. S. C. B. Mannsfeld, A. Virkar, C. Reese, M. F. Toney and Z. Bao, *Adv. Mater.*, 2009, **21**, 2294-2298.
21. U. H. F. Bunz, *Acc. Chem. Res.*, 2015, **48**, 1676-1686.
22. J. E. Anthony, *Chem. Rev.*, 2006, **106**, 5028-5048.
23. Z.-F. Yao, J.-Y. Wang and J. Pei, *Cryst. Growth Des.*, 2018, **18**, 7-15.
24. K. J. Thorley, T. W. Finn, K. Jarolimek, J. E. Anthony and C. Risko, *Chem. Mater.*, 2017, **29**, 2502-2512.
25. K. A. McGarry, W. Xie, C. Sutton, C. Risko, Y. Wu, V. G. Young, J.-L. Brédas, C. D. Frisbie and C. J. Douglas, *Chem. Mater.*, 2013, **25**, 2254-2263.
26. J. Li, M. Wang, S. Ren, X. Gao, W. Hong, H. Li and D. Zhu, *J. Mater. Chem.*, 2012, **22**, 10496-10500.
27. G. R. Llorente, M.-B. Dufourg-Madec, D. J. Crouch, R. G. Pritchard, S. Ogier and S. G. Yeates, *Chem. Commun.*, 2009, 3059-3061.
28. J. E. Anthony, D. L. Eaton and S. R. Parkin, *Org. Lett.*, 2002, **4**, 15-18.
29. U. H. F. Bunz, J. U. Engelhart, B. D. Lindner and M. Schaffroth, *Angew. Chem. Int. Ed.*, 2013, **52**, 3810-3821.
30. Y. Tsutsui, G. Schweicher, B. Chattopadhyay, T. Sakurai, J.-B. Arlin, C. Ruzié, A. Aliev, A. Ciesielski, S. Colella, A. R. Kennedy, V. Lemaury, Y. Olivier, R. Hadji, L. Sanguinet, F. Castet, S. Osella, D. Dudenko, D. Beljonne, J. Cornil, P. Samori, S. Seki and Y. H. Geerts, *Adv. Mater.*, 2016, **28**, 7106-7114.
31. M. J. Kang, E. Miyazaki, I. Osaka, K. Takimiya and A. Nakao, *ACS Appl. Mater. Interfaces*, 2013, **5**, 2331-2336.
32. C. A. Hunter and J. K. M. Sanders, *J. Am. Chem. Soc.*, 1990, **112**, 5525-5534.
33. C. Wang, H. Nakamura, H. Sugino and K. Takimiya, *Chem. Commun.*, 2017, **53**, 9594-9597.
34. K. Takimiya, S. Shinamura, I. Osaka and E. Miyazaki, *Adv. Mater.*, 2011, **23**, 4347-4370.
35. C. Sutton, C. Risko and J.-L. Brédas, *Chem. Mater.*, 2016, **28**, 3-16.
36. S. M. Ryno, C. Risko and J.-L. Brédas, *Chem. Mater.*, 2016, **28**, 3990-4000.
37. I. Yavuz, B. N. Martin, J. Park and K. N. Houk, *J. Am. Chem. Soc.*, 2015, **137**, 2856-2866.
38. R. A. Krawczuk, S. Tierney, W. Mitchell and J. J. W. McDouall, *Faraday Discuss.*, 2014, **174**, 281-296.
39. S. I. Stupp and L. C. Palmer, *Chem. Mater.*, 2014, **26**, 507-518.
40. D. Philp and J. F. Stoddart, *Angew. Chem. Int. Ed. Eng.*, 1996, **35**, 1154-1196.
41. L.-C. Wang and Q.-Y. Zheng, in *Hydrogen Bonded Supramolecular Structures*, eds. Z.-T. Li and L.-Z. Wu, Springer Berlin Heidelberg, Berlin, Heidelberg, 2015, pp. 69-113.
42. E. D. Głowacki, M. Irimia-Vladu, M. Kaltenbrunner, J. Gsiorowski, M. S. White, U. Monkowius, G. Romanazzi, G. P. Suranna, P. Mastrolilli, T. Sekitani, S. Bauer, T. Someya, L. Torsi and N. S. Sariciftci, *Adv. Mater.*, 2013, **25**, 1563-1569.
43. E. D. Glowacki, M. Irimia-Vladu, S. Bauer and N. S. Sariciftci, *J. Mater. Chem. B*, 2013, **1**, 3742-3753.
44. C. Zhu, A. U. Mu, Y.-H. Lin, Z.-H. Guo, T. Yuan, S. E. Wheeler and L. Fang, *Org. Lett.*, 2016, **18**, 6332-6335.
45. E. Moulin, J.-J. Cid and N. Giuseppone, *Adv. Mater.*, 2013, **25**, 477-487.

46. H. Zhang, R. Deng, J. Wang, X. Li, Y.-M. Chen, K. Liu, C. J. Taubert, S. Z. D. Cheng and Y. Zhu, *ACS Appl. Mater. Interfaces*, 2017, **9**, 21891-21899.
47. Y. Zou, T. Yuan, H. Yao, D. J. Frazier, D. J. Stanton, H.-J. Sue and L. Fang, *Org. Lett.*, 2015, **17**, 3146-3149.
48. J. Dhar, D. P. Karothu and S. Patil, *Chem. Commun.*, 2015, **51**, 97-100.
49. Z. He, D. Liu, R. Mao, Q. Tang and Q. Miao, *Org. Lett.*, 2012, **14**, 1050-1053.
50. D. Yokoyama, H. Sasabe, Y. Furukawa, C. Adachi and J. Kido, *Adv. Funct. Mater.*, 2011, **21**, 1375-1382.
51. W. Hong, Z. Wei, H. Xi, W. Xu, W. Hu, Q. Wang and D. Zhu, *J. Mater. Chem.*, 2008, **18**, 4814-4820.
52. L.-C. Campeau, M. Parisien, A. Jean and K. Fagnou, *J. Am. Chem. Soc.*, 2006, **128**, 581-590.
53. M. E. Budén, V. A. Vaillard, S. E. Martin and R. A. Rossi, *J. Org. Chem.*, 2009, **74**, 4490-4498.
54. R. O. Loutfy, *J. Chem. Phys.*, 1977, **66**, 4781-4787.
55. R. Cernini, X. C. Li, G. W. C. Spencer, A. B. Holmes, S. C. Moratti and R. H. Friend, *Synth. Met.*, 1997, **84**, 359-360.
56. E. Clar, *The aromatic sextet*, J. Wiley, 1972.
57. The distance between the pyrrole and pyridine nitrogen atoms is given due to the limited accuracy of the hydrogen atoms positioning from the X-ray diffraction data.
58. E. F. Paulus, F. J. J. Leusen and M. U. Schmidt, *CrystEngComm*, 2007, **9**, 131-143.
59. M. D. Curtis, J. Cao and J. W. Kampf, *J. Am. Chem. Soc.*, 2004, **126**, 4318-4328.
60. M. A. Spackman and D. Jayatilaka, *CrystEngComm*, 2009, **11**, 19-32.
61. Hirshfeld surface analysis was done using the software Crystal Explorer 2.1, S. K. Wolff, D. J. Grimwood, J.J. McKinnon, D. Jayatilaka, M. A. Spackman. University of Western Australia (2007)
62. J. J. McKinnon, D. Jayatilaka and M. A. Spackman, *Chem. Commun.*, 2007, 3814-3816.
63. M. A. Spackman and J. J. McKinnon, *CrystEngComm*, 2002, **4**, 378-392.
64. K.-J. Baeg, Y.-Y. Noh, J. Ghim, B. Lim and D.-Y. Kim, *Adv. Funct. Mater.*, 2008, **18**, 3678-3685.
65. C. Liu, Y. Xu and Y.-Y. Noh, *Mater. Today*, 2015, **18**, 79-96.
66. Z. Wang, M. W. Alam, Y. Lou, S. Naka and H. Okada, *Appl. Phys. Lett.*, 2012, **100**, 043302.
67. D. Berg, C. Nielinger, W. Mader and M. Sokolowski, *Synth. Met.*, 2009, **159**, 2599-2602.
68. Y. Hiroyuki, M. Jin, A. Shinji and S. Yoshimasa, *Jpn. J. Appl. Phys.*, 2008, **47**, 4728.
69. H. Li, C. Li, L. Duan and Y. Qiu, *Isr. J. Chem.*, 2014, **54**, 918-926.
70. C. D. Sheraw, T. N. Jackson, D. L. Eaton and J. E. Anthony, *Adv. Mater.*, 2003, **15**, 2009-2011.
71. J. L. Brédas, J. P. Calbert, D. A. da Silva Filho and J. Cornil, *Proc. Natl. Acad. Sci.*, 2002, **99**, 5804-5809.
72. H.-Z. Gao, *Int. J. Quantum Chem.*, 2012, **112**, 740-746.
73. It is assumed that transfer integrals might be subject to a certain variation depending on the density functional (ref. 70)
74. Parr, R. G.; Yang, W. *Density functional theory of atoms and molecules*. Oxford University Press, N. Y. 1989.
75. A. D. Bochevarov, E. Harder, T. F. Hughes, J. R. Greenwood, D. A. Braden, D. M. Philipp, D. Rinaldo, M. D. Halls, J. Zhang and R. A. Friesner, *Int. J. Quantum Chem.*, 2013, **113**, 2110-2142.
76. Schrödinger Release 2016-4: Jaguar, Schrödinger, LLC, New York, NY, 2016.
77. X. Wang and K.-C. Lau, *J. Phys. Chem. C*, 2012, **116**, 22749-22758.
78. C. Sutton, J. S. Sears, V. Coropceanu and J.-L. Brédas, *J. Phys. Chem. Lett.*, 2013, **4**, 919-924.
79. E. Livshits and R. Baer, *Phys. Chem. Chem. Phys.*, 2007, **9**, 2932-2941.
80. R. Baer and D. Neuhauser, *Phys. Rev. Lett.*, 2005, **94**, 043002.
81. Z.-Q. You, Y.-C. Hung and C.-P. Hsu, *J. Phys. Chem. B*, 2015, **119**, 7480-7490.
82. Q. Wu and T. Van Voorhis, *Phys. Rev. A*, 2005, **72**, 024502.
83. Materials Science Suite 2016-4, Schrödinger, LLC, New York, NY, 2016
84. Schrödinger Release 2016-4: Maestro, v., Schrödinger, LLC, New York, NY, 2016.